Available online at www.sciencedirect.com
SCIENCE DIRECT®

Journal of the European Ceramic Society 23 (2003) 2787–2796
www.elsevier.com/locate/jeurceramsoc

Wetting and strength issues at Al/α–alumina interfaces

E. Saiz[a,*], A.P. Tomsia[a], K. Suganuma[b]

[a]*Materials Sciences Division, Lawrence Berkeley National Laboratory, University of California, Berkeley, CA 94720, USA*
[b]*Institute of Scientific and Industrial Research, Osaka University, Japan*

Abstract

The wetting behavior and strength at aluminum/alumina interfaces is an active subject of research. Al/alumina applications include ceramic-metal composites and several applications for electronic industries. In this paper the interface strength and microstructure of Al/α-alumina was investigated. We discovered that, in a solid-state joining, the strength of the joint increases with increasing joining temperature, whereas, in a liquid-state joining, the strength of the joint gradually decreases with increasing temperature due to the formation of unbonded areas. The strength, σ_b, is expressed by the following equation as a function of unbonded area, A: $\sigma_b = 2.69\ A + 116$ ($70\% \leqslant A \leqslant 100\%$). The highest strength reached 400 MPa when the interface was formed around the melting temperature of aluminum. An aluminum layer close to the interface became a single crystal when it was bonded to a sapphire. The following crystallographic orientation relationship was established:

$$\left(\bar{1}11\right)_{Al}//(001)_{\alpha-Al_2O_3},\ <110>_{Al}\ //\ <100>_{\alpha-Al_2O_3}$$

Amorphous alumina islands were formed at the interface. In the amorphous alumina, γ-alumina nanocrystals grew from the sapphire, with the same orientation relationship to sapphire as above.

Keywords: Alumina; Aluminum; Interface; Microstructure; Sapphire; Strength

1. Introduction

The combination of alumina and aluminum is well known and has many applications. For instance, α-alumina has been used in the electronic industry for many years as a ceramic insulator, whereas aluminum is one of the best electrodes, having good electric conductivity, second only to copper. Powders and fibers of alumina are also used to reinforce aluminum alloys, one of the most common lightweight materials for components in automobile engines and other transportation systems. In many of these cases, the formation of a strong aluminum/alumina interface is required. Consequently, extensive research is being performed on the wetting of liquid aluminum on alumina and on the joining and brazing of both materials.[1–10]

The aim of this work is to evaluate the basic parameters that govern the formation of aluminum/alumina interfaces. Sessile drop experiments have been performed to study the wetting of liquid aluminum on alumina. The interfacial microstructure has been evaluated using atomic force microscopy (AFM), scanning electron microscopy (SEM), and transmission electron microscopy (TEM). The evolution of the interfacial morphology was followed in order to determine the relevant atomic transport rates. The strength of aluminum/alumina bonds fabricated at various temperatures using solid-state diffusion bonding or liquid-state brazing was measured and correlated to the interfacial microstructure.

2. Experimental procedure

2.1. Wetting experiments

Wetting experiments were performed by melting small pieces (0.2–0.5 g) of Al (99.999%, Johnson Mattey) on sapphire and polycrystalline alumina substrates. The experiments were conducted in vacuum or Ar (gettered

* Corresponding author. Tel.: +1-510-486-1446; fax: +1-510-486-4761.
E-mail address: esaiz@lbl.gov (E. Saiz).

0955-2219/03/$ - see front matter © 2003 Elsevier Ltd. All rights reserved.
doi:10.1016/S0955-2219(03)00290-5

at 800 °C with Ti–Zr chips, $p(O^2) \sim 10^{-19}$ atm) in a resistance furnace with a Ta heating element. Heating rates varied from 10 to 35 °C/min. After the required time at a given temperature, the furnace was shut off, leading to faster cooling rates. The contact angles of molten aluminum were measured (±2°) as a function of time and temperature by viewing through a porthole in the furnace. Experiments in gettered Ar were also performed by placing the sample in a closed alumina crucible. It is expected that under these conditions, the $p(O_2)$ inside the crucible would be close to the phase boundary value at which Al and Al_2O_3 can coexist in equilibrium, $p(O_2)^{eq}$. In these experiments, the contact angles were measured after cooling. Our experience indicates that the contact angles measured right before and after cooling are different only by a few degrees.

The polycrystalline alumina substrates were prepared from pure Al_2O_3 powders (99.999%, Showa-Denko, Japan). The powders were isostatically pressed (200 MPa), and the resulting blocks were embedded in pure alumina powder and sintered in vacuum (10^{-3} Pa) at 1700 °C for 2 h. Substrates (~10×10×2 mm) were cut from the sintered block using a diamond saw and polished with diamond paste (1 μm particle size). Subsequently, they were annealed in vacuum at 1600 °C for 6 h in order to ensure that the grain boundaries intersected the surface at their equilibrium angle. The final average grain size was ~20 μm. In order to minimize contamination during annealing, the substrates were placed with the polished sides face to face and embedded in pure alumina powder. The boundary grooves that formed during heat treatment were removed by a light polishing with diamond (1 μm particle size).

After the wetting tests, the aluminum was dissolved from the substrate with HCl and the area under the drop analyzed by optical microscopy, SEM, and AFM. The profiles of the boundary grooves at the solid/liquid and solid/vapor interfaces were measured using AFM line analysis in the constant-force mode. In order to study the evolution of grooves with time, pieces of the aluminum were consecutively melted at the same place on the substrate and the interface was analyzed after sequential heating and etching steps. Parallel studies of boundary grooving on free alumina substrates were performed at the same temperatures and atmospheres.

2.2. Joining experiments

A number of α-alumina disks of 50 mm diameter and 20 mm height were sintered by hot-pressing alumina powder (average particle size of 0.3 μm, Sumitomo Chemical Co., Ltd., AKP30) under 30 MPa pressure at 1450 °C for 1 h in an Ar atmosphere. From those disks, 16×16×18 mm blocks were cut. The faces to be joined (16×16 mm) were ground and polished to have optical flatness. Bars (3×4×35 mm) were cut from the sintered body, and their strength was measured using the four-point bending test. The average alumina strength was 551 MPa (standard deviation 43 MPa). Sapphire was also used for bonding to aluminum to characterize the interfacial structure. The bonding face was the (001) basal plane of α-alumina.

Joining specimens were prepared by inserting two aluminum sheets (99.993%, 100 μm thick) between two alumina blocks and hot pressing in a vacuum maintained at $1.5 \cdot 10^{-3}$ Pa pressure. The joining temperatures varied between 550 °C (solid-state diffusion bonding) and 1200 °C (liquid-state brazing). The applied pressure and holding time were 10 MPa and 1 h, respectively.

From the bonded blocks, 3×4×36 mm bars were cut and used for measuring the joining strength by four-point bending at room temperature. Cross-head speed was 0.5 mm/min. The upper span and lower span were 10 and 30 mm, respectively.

The interfacial microstructure was characterized primarily by TEM. TEM specimens (disks 200 μm thick and 2.3 mm in diameter) were cut from the joints, dimpled, and polished by Ar ion thinning. The specimens were coated with a thin carbon layer to avoid charging. For high resolution, a JEOL JEM200CX microscope was used at 200 kV; and for nano-EDS analysis, a HITACHI HF2000 was used at the same voltage.

3. Results and discussion

3.1. Wetting and diffusion studies

The effect of temperature on the final contact angle of molten Al on alumina substrates is illustrated in Fig. 1, where results taken from the literature[1,11–16] are also presented for comparison. There is no significant difference in the angles recorded on sapphire or polycrystalline alumina. Below 1000 °C, the drop is covered by a thick oxide layer and exhibits an irregular shape. At temperatures higher than 1000 °C, the drop is shiny, and the contact angle (θ) decreases as time and temperature increase, approaching a value of ~70° after 60 min at 1400 °C. In experiments performed under vacuum at temperatures higher than 1100 °C, the contact angle of aluminum oscillates periodically. For example, at 1100 °C, after reaching a value of ~80°, θ decreases in ~20–30 min to ~60° and then suddenly jumps again to the maximum value. In these cases, after removing the drops, rings are visible on the alumina surface, one for each jump (Fig. 2).

The Al/Al_2O_3 system has a fundamental difference with respect to other metal/oxide combinations: at a given temperature there is only one oxygen partial pressure at which Al and Al_2O_3 can coexist in equilibrium [$p(O_2)^{eq}$]. This oxygen partial pressure, ranging from $\sim 10^{-59}$ atm at 600 °C to $\sim 10^{-22}$ atm at 1500 °C,

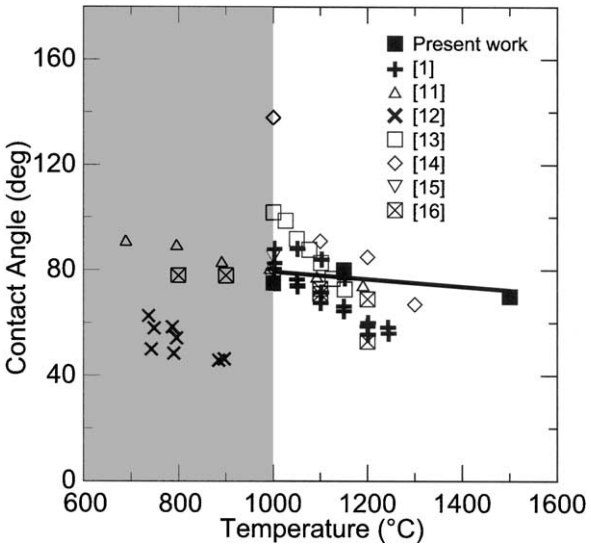

Fig. 1. Contact angles of Al drops on alumina. The results from the present work were obtained after 60 min at the experimental temperature. Results from other authors are also presented for comparison. Because the Al drop is usually covered by an oxide layer at temperatures below 1000 °C (gray area in the graph), the data in that range correspond to experiments performed using a doser or other means to produce a pristine Al surface.

is typically much lower than that attainable in most experimental setups. For other metal/ceramic systems, there is an adequate range of $p(O_2)$ where both phases can coexist in equilibrium, and a region can exist in which all the interfaces are stoichiometric, and consequently the interfacial energies are independent of oxygen activity. However, in the Al/Al_2O_3 system, some adsorption is expected at all the interfaces involved. For example, as with other metals, adsorption of oxygen can be expected on the surface of the liquid aluminum in equilibrium with its oxide. Consequently, the surface energy of Al at $p(O_2)^{eq}$ will be somewhat lower than that of pure, clean Al.

The low value of the equilibrium $p(O_2)$ explains the stability of the oxide layer on the liquid surface at temperatures below 1000 °C. At higher temperatures this oxide layer disappears. Three reasons have been proposed for this behavior: erosion through formation of volatile Al_2O species,[17,18] cracking due to the volume changes, and thermal expansion mismatch.[17] When the temperature increases above 1000 °C, the Al vapors react with the oxygen such that the oxygen activity around the drop will correspond to the equilibrium value for the Al/Al_2O_3 system.[17,18] The observed oscillation of the contact angle in vacuum at high temperatures is associated with the formation of ridges at the triple line. The ridges form to achieve full three-dimensional equilibrium of the surface forces at the triple junction.[19,20] After the formation of the ridge, the fast evaporation of Al decreases the contact angle below a critical value, and the junction breaks away from the ridge.[20] Afterwards, a new ridge forms and the cycle starts again. According to this description, the maximum value of the contact angle, after each jump, should correspond to the one described by Young's equation.[19,20]

The AFM and SEM analyses of the alumina surface after the metal dissolved show that the Al/Al_2O_3 interfaces are strongly faceted (Fig. 3). The shape of some

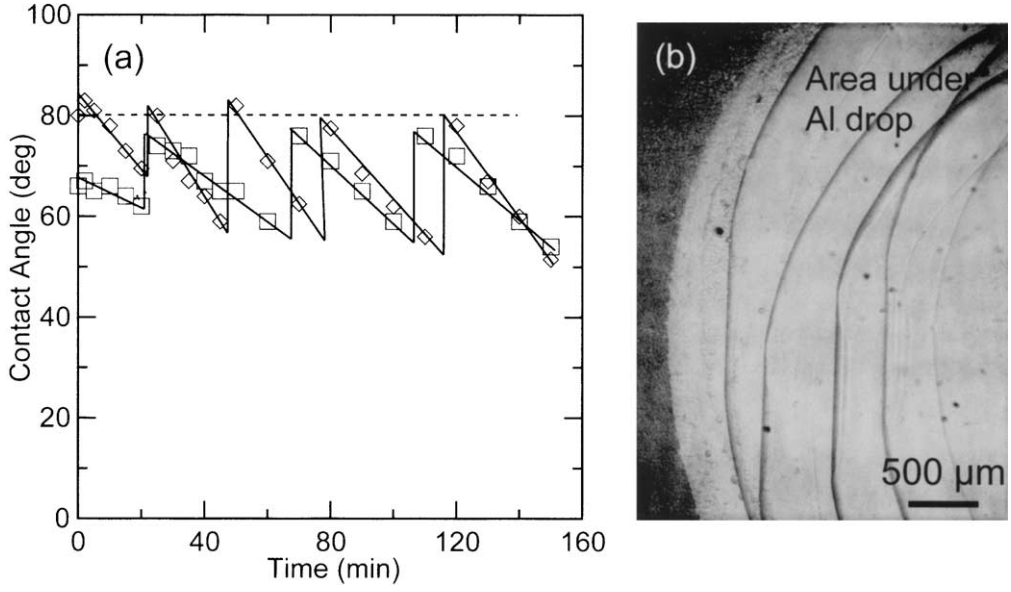

Fig. 2. (a) The oscillation of the macroscopic contact angles for Al/Al_2O_3 in vacuum at 1100 °C is due to the combined effects of rapid evaporation and successive formation and breakaway from ridges that pin the periphery. The dotted line shows the equilibrium contact angle described by Young's equation. (b) Optical micrograph of the "reaction rings" that can be observed after removing the Al drop; the rings are actually delineated by triple-line ridges.

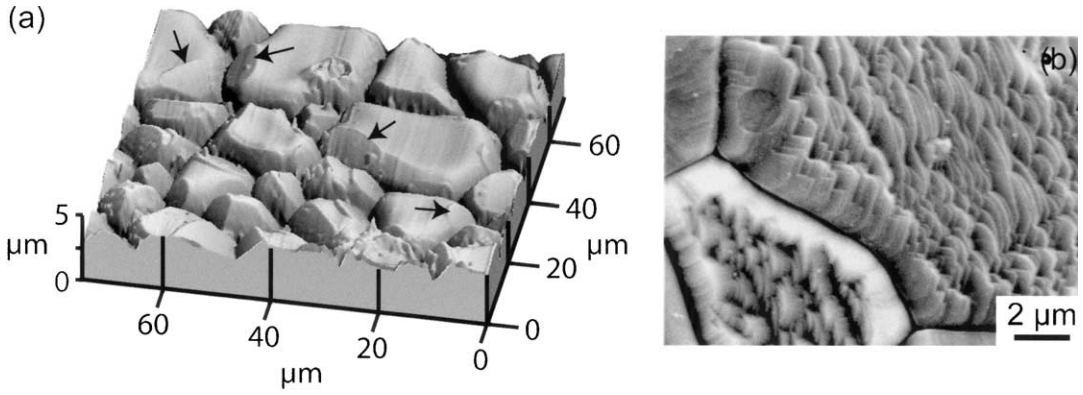

Fig. 3. (a) AFM micrograph of the area of the alumina substrate that was under an Al drop melted for 15 min at 1500 °C. (b) SEM micrograph of the area under a drop melted for 30 min at 1100 °C. Facets are clearly visible (marked with arrows on the AFM image).

facets suggests that the alumina basal plane is one of the low-energy surfaces. The shapes of the interfacial grain-boundary grooves correspond to diffusion-controlled growth, albeit perturbed by the facets. This is in contrast to the stoichiometric interfaces between alumina and other fcc metals that appear to be very isotropic.[21] The Al_2O_3 surfaces outside the Al drops seem to be less strongly faceted than those under the Al drops, but somewhat more so than stoichiometric alumina surfaces of Al_2O_3. Mass transport is orders of magnitude faster than at the Ni, Au, or Cu/Al_2O_3 interfaces at similar temperatures.[21]

The measurement of groove angles and the liquid–solid contact angle allowed the deduction of relevant interfacial energies (Table 1). Annealing at 1500 °C in a closed alumina crucible produced a clean Al drop, suggesting that the equilibrium $p(O_2)$ was achieved. There is some degree of uncertainty in the reported γ_{lv} due to the low oxygen activities needed to maintain molten Al free of oxide.[22,23] To account for these uncertainties, two calculations are presented in Table 1: one used 80° and 0.7 J/m^2, which are upper bounds for the coexistence condition at 1500 °C; and the other used 70° and 0.3 J/m^2, which may be on the low side of better estimates for this condition. The lower values are consistent with the expected decrease of the surface energy of the metal at the oxygen partial pressure in which it coexists with its own oxide with respect to reported values for clean aluminum; this decrease is due to oxygen adsorption.[21] For both sets, the resulting γ_{sv} is unambiguously lower, and γ_{gb} is somewhat smaller than reported for stoichiometric interfaces in metal/alumina systems (γ_{sv} 1.1–1.2 J/m^2, γ_{gb}=0.8–1.1 J/m^2).[21] This can be expected if there is some adsorption. For either value of θ, a higher value of γ_{lv}, than that chosen for Al in equilibrium with Al_2O_3 would yield surface and grain-boundary energies for alumina higher than those for stoichiometric interfaces, which is very unlikely. Instead, application of the Gibbs adsorption isotherm would indicate that if these surfaces were oxygen-deficient (i.e. having an Al excess), these energies should be lower.[21,22] As the solid–vapor and especially the solid–liquid interfaces are faceted, torque terms can be important, and some corrections must be applied[24,25] in order to calculate each interfacial energy exactly; the values in Table 1 assume that the average energies remain approximately correct.

Table 1
Measured contact and dihedral angles and corresponding interfacial energies corresponding to experiments performed at 1500 °C[a]

	θ	ϕ_l	ϕ_v	γ_{lv} (J/m^2)	γ_{sl} (J/m^2)	γ_{sv} (J/m^2)	γ_{gb} (J/m^2)
Lower bound	70°	93°	107°	0.30[15]	0.65	0.76	0.90
Upper bound	80°[15]	–	–	0.74[31]	0.81	0.95	1.12

[a] The dihedral angles have been measured from the AFM profiles and include corrections due to the finite AFM tip radius[21] Two sets of calculations are presented, representing lower and upper bounds for the coexistence condition.

The transport rates observed at the Al/Al_2O_3 interfaces and free alumina surface away from the aluminum drop are much faster than any ever reported for alumina surfaces, implying much faster diffusivities. It should be pointed out that most of the surface and volume diffusivities reported for alumina have been calculated after experiments performed at oxygen partial pressures far higher than the one at which aluminum and alumina can coexist in equilibrium. Although vapor transport may be suspected to control groove growth on the free alumina surface ahead of the aluminum drop at higher temperatures, the implied $t^{1/2}$ fit was unsatisfactory.[26] Groove growth involves diffusion of both Al and O ions. Although each species could move independently, the dissolution and deposition must involve stoichiometric Al_2O_3. Typically, experiments performed on alumina surfaces are done at oxygen partial pressures where the groove growth is controlled by the surface diffusion of Al ions. Due to the low oxygen activity in the Al/Al_2O_3 system, the calculated interface diffusivity on the alumina surface ahead of the aluminum

drop would likely represent that for O instead of Al, and is for an Al-rich interface.

At the solid/liquid interface, comparison of $t^{1/3}$ (groove growth controlled by volume diffusion),[27] $t^{1/4}$ (groove growth controlled by interfacial diffusion),[20] and combined fittings (which add the contributions for both paths)[21] for the evolution of groove width with time do not clearly favor any one diffusion path, suggesting that both are contributing to groove growth (Table 2). The upper limit for the interfacial diffusivity ($t^{1/4}$ fitting) and the value from the combined equation are similar. The corresponding interfacial diffusivities at the metal/ceramic interface are somewhat similar to those measured on the alumina surface ahead of the Al drop (taking into account the temperature difference). The fast volume diffusivities are consistent with transport through the liquid phase. In this case, the diffusion of the species (Al, O, or some complexes of them) with the lower xD_v product (where x is the molar solubility and D_v the volume diffusivity) will control grooving kinetics. Since transport in the liquid depends on the concentration of diffusing species, it could be expected that diffusion of O or O-rich species should be limiting at very low oxygen activity at which aluminum and alumina can coexist in equilibrium. The implied solubilities of O in the liquid Al (10^{-5}–10^{-7}) are reasonable.[28]

The basal plane has clearly become relatively more stable for the interface, and seemingly also for the surface of the alumina ahead of the aluminum drop. This indicates that there is a change in the Wullf plot for the sapphire–vapor surface versus those recently reported for higher oxygen activities;[29,30] this change is consistent with the idea that the surfaces oriented parallel to alternating sheets of O and Al atoms in the crystal structure may be partially reduced more readily. The (001) plane has been shown to become Al-rich in ultra-high vacuum.[31,32] Evidently, the situation is analogous for the Al/Al_2O_3 interface. The average surface and grain boundary energies are reduced somewhat with respect to those recorded for other metals at higher $p(O_2)$. For the surface, this would reflect the lower energy for surfaces nearly parallel to (001), but other surfaces may be susceptible to reduction to a lesser degree. Evidently, at least some grain boundaries are similarly susceptible to becoming Al-rich.

3.2. Interface strength

Fig. 4 shows the bending strength of the alumina joints as a function of joining temperature. Data taken from the literature are also included for comparison.[33,34] The bonding strength is low for the joint solid-state-bonded at 550 °C, but it increases as the temperature rises to 650 °C, and peak strength is achieved at joining temperatures between 650 and 700 °C. Above 700 °C, the strength gradually decreases as the joining temperature increases. The peak bond strength is about 450 MPa, much higher than aluminum (~100 MPa) and approximately 80% of the alumina strength. In fact, some of the joints fractured in alumina away from the interfacial region.

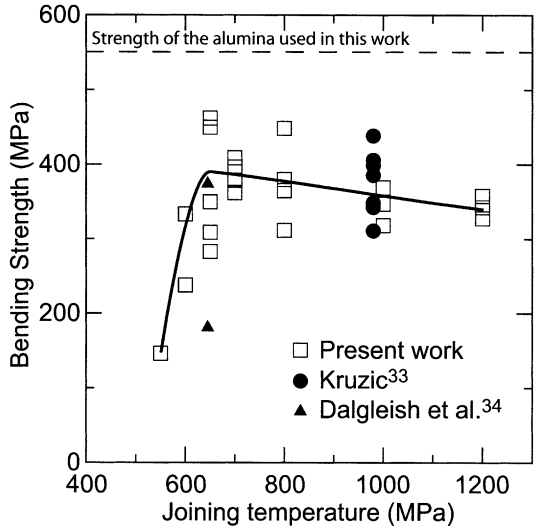

Fig. 4. Bending strength of alumina/aluminium/alumina joints as a function of joining temperature. Results from other authors are also presented for comparison. The strength depends on the thickness of the aluminum foil; stronger bonds are achieved for a given temperature with thinner Al layers.

Table 2
Surface, volume, and combined (surface and volume) diffusivities calculated for the Al/Al_2O_3 system[a]

System	Temp.(°C)	Surface diffusion $w = 4.6\left(\frac{B_i t}{2}\right)^{1/4} + w_0$		Volume diffusion $w = 5\left(\frac{B_v t}{2}\right)^{1/3} + w_0$		Combined $w = 4.6\left(\frac{B_i t}{2}\right)^{1/4} + 5\left(\frac{B_v t}{2}\right)^{1/3} + w_0$		
		$\omega \cdot D_i$ ($m^3 \cdot s$)	w_0 (nm)	$x \cdot D_v$ ($m^2 \cdot s$)	w_0 (nm)	$\omega \cdot D_i$ ($m^3 \cdot s$)	$x \cdot D$,($m^2 \cdot s$)	w_0(nm)
Al_2O_1	1600	$4.6 \cdot 10^{-21}$	0					
Al_2O_3 (Al)	1500	$2.6 \cdot 10^{-18}$	2688					
Al/Al_2O_3	1100	$1.1 \cdot 10^{-19}$	−162	$5 \cdot 10^{-14}$	630	$4.1 \cdot 10^{-20}$	$6.6 \cdot 10^{-16}$	0

[a] The Al_2O_3(Al) values correspond to the surface of alumina outside of the aluminum drop (experiment performed in a closed crucible). The Al/Al_2O_3 values correspond to the metal/ceramic interface. Values for the clean surface of alumina (without Al present in the system) measured using the AFM technique are also presented for comparison. In the mathematical fittings, w is the groove width, $B_i = (\omega D_i \gamma_i \Omega)/kT$ and $B_v = (xD_v \gamma_i \Omega)/kT$, Ω is the molecular volume, ω is the interfacial width, x is the molar solubility in the liquid metal for the diffusing species and D_i and D_v are the interfacial and volume diffusivities; γ_i is the corresponding interfacial energy, and k is the Boltzman constant.

When evaluating the strength of ceramic/metal joints, several parameters related to the difference in elastic and plastic properties of the two materials should be considered. The plastic and elastic deformation of the metal layer becomes large with increasing thickness. Inverse thickness dependence has been attributed to the influence of corner stress concentrations. A thicker metal layer yields a larger zone of high stress acting on the flaw population.[34] Because the analytical equations for four-point and three-point bending strengths are derived for bars with uniform curvature, a large deviation between the measured and absolute strengths for ceramic/metal joints can occur. The final thickness of the metal layer varied with joining temperature (Fig. 5), which may influence strength. Below the melting temperature of aluminum, 660 °C, the thickness of the aluminum layer was about 100 μm, but it decreased to about 10 μm after liquid-state bonding, almost remaining constant up to 1200 °C.

Joints fabricated in the low-temperature range, between 550 and 600 °C, exhibited interface decohesion at the aluminum/alumina interface. In contrast, joints formed at 650 °C did not show any interface decohesion but showed cracks inside the aluminum layer or in the alumina. This observation implies that the interface strength is higher than 400 MPa. Thus, these joints are different in both strength and fracture mode, even though the thickness of the aluminum layer is almost the same. The weak strength of the joints fabricated in the lower temperature range can be attributed to the presence of an oxide skin on the aluminum. As the temperature approaches the melting point of aluminum, the oxide skin breaks, and aluminum and alumina can form a direct interface with high strength.

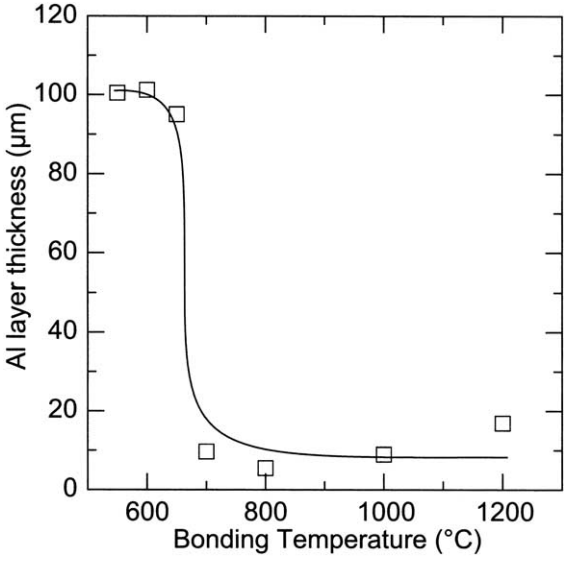

Fig. 5. Thickness of aluminum layer as a function of bonding temperature.

Above the Al melting point, the final thickness of the interlayer (~10 μm) does not depend on the joining temperature. The gradual decrease in strength with temperature above 660 °C is not a result of variations in the thickness of the aluminum layer but a result of the development of unbonded regions on the joint. Fig. 6 shows typical fracture surfaces after bending tests (the fracture propagated from the bottom to the top). The fracture surface of the sample bonded just above the melting temperature of aluminum, 700 °C, shows a crack that propagated in the aluminum layer up to the middle of the bar and then moved into the alumina body. In the aluminum fracture surface, no defects, such as unbonded areas, are observed. In contrast, joints fabricated at higher temperature exhibit many large unbonded areas. Fig. 7 shows the total bonded area on the fracture surface as a function ofjoining temperature. The ratio of bonded area to the total interface area gradually decreases from ~100% at 700 °C to ~70% at 1200 °C. Surprisingly, the joints with 30% unbonded area still exhibit high strength (~90% of the maximum strength obtained at 650–700 °C). The relationship between strength and unbonded area, replotted in Fig. 8, is almost linear. The following experimental relationship can be derived by the least-squares method:

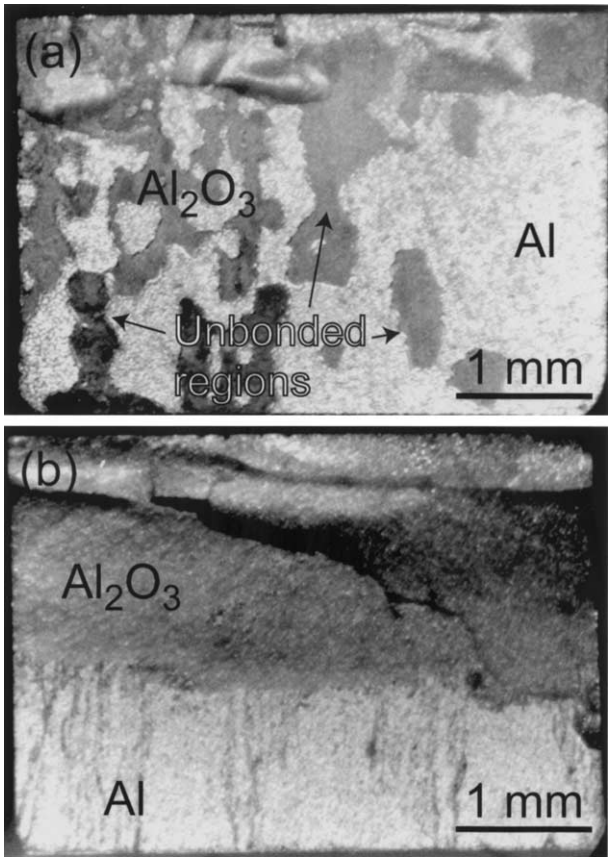

Fig. 6. Fracture surface of joints bonded at 1200 °C (a) and at 700 °C (b). The fracture proceeded from the bottom to the top.

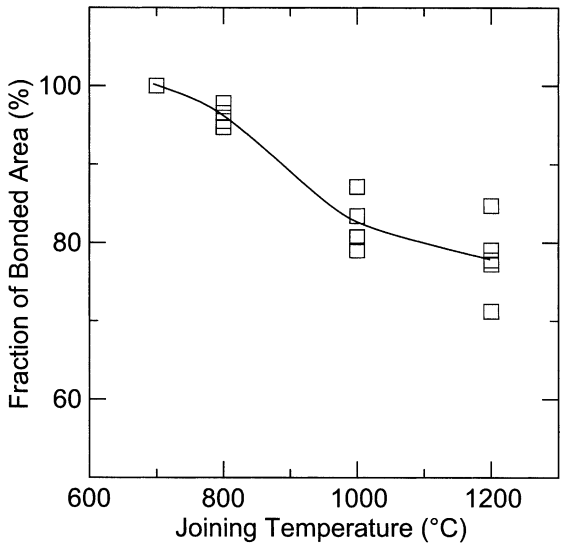

Fig. 7. Change in the fraction of the bonded area on the fracture surface as a function of bonding temperature.

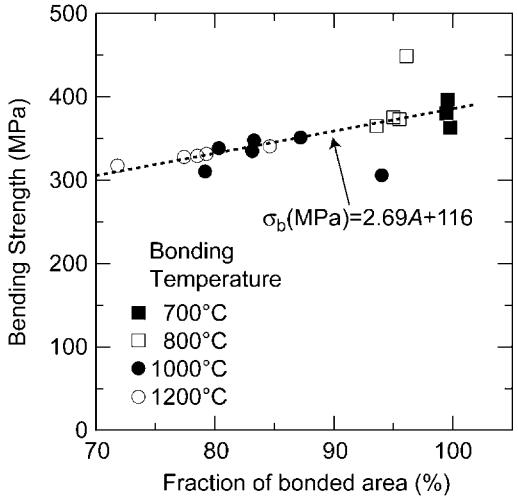

Fig. 8. Bending strength of each specimen as a function of fraction of bonded area.

$$\sigma_b = 2.69A + 116 \quad (1)$$

where σ_b is the bending strength of a joint in MPa and A is the ratio of bonded arealtotal interface area. It should be noted that when A is zero, the strength is 116 MPa. The equation is, therefore, valid for $A \geqslant 70\%$, which is the smallest bonded area measured.

The decreasing strength with increasing joining temperature can be explained by taking into account aluminum wetting and viscosity. With increasing temperature, contact angle and viscosity of the liquid Al decreases. Because the contact angle of Al on Al_2O_3 is lower than 90°, the capillary pressure drives the alumina blocks tighter when an external pressure is also applied. However, most of the melt will be squeezed out of the joint layer, leading to the formation of unbonded regions. With increasing temperature, the movement of the molten aluminum towards the free surface becomes faster as the viscosity and contact angle decrease, resulting in larger unbonded areas.

Even though unbonded regions remain at the interface, the strength of the bond is quite high, reaching almost 80% of the alumina strength. In some cases, fracture occurred inside the alumina, away from the interface, from which we can infer that the interfacial aluminum/alumina strength is very high. Thus, we can conclude that aluminum brazes are very useful for joining aluminum and alumina for structural applications, which is why aluminum alloy matrix composites have strong interfaces between matrices and various alumina reinforcements when good wetting and direct contact are achieved between both phases.

3.3. Aluminum/alumina interface

Aluminum and alumina form quite a strong interface. The α–alumina oxide is the most stable oxide of aluminum, and the phase diagram indicates that no other compound can be formed at the Al/Al_2O_3 interface.[35] This observation was confirmed by TEM of the polycrystalline alumina joint. To better characterize the Al/Al_2O_3 interface, aluminum/sapphire joints were fabricated at 650 °C, the temperature at which the highest strength was obtained for the aluminum/polycrystalline alumina system.

The interface was studied by TEM. Fig. 9 shows a TEM micrograph of the interface with the diffraction patterns of sapphire and aluminum. The incident electron beam is located along the $<100>$ direction of sapphire, and the bonding face, which is the basal plane of sapphire, i.e. (001), is viewed edge-on. The interface is flat, without any modification by the bonding procedure. Polycrystalline in its initial state, aluminum becomes a single crystal without any boundary inside. Several points were analyzed, and all areas had the same crystallographic characteristics. The following orientation relationship was derived from the diffraction patterns:

$$\left(\bar{1}11\right)_{Al}//(001)_{\alpha-Al_2O_3}, <110>_{Al} //<100>_{\alpha-Al_2O_3} \quad (2)$$

This orientation relationship has been reported for interfaces between fcc metals and sapphire.[36,37] At these interfaces, sixfold symmetric close-packed atomic arrangements facing together provide the best periodicity match. However, the lattice mismatch between the (111) plane of aluminum and the (001) plane of alumina is quite large, up to 20.8%. As shown in the diffraction pattern in Fig. 9 and the lattice images in Figs. 10 and 11, both crystals incline or rotate with respect to each other slightly, which should relax the large mismatch at the interface.

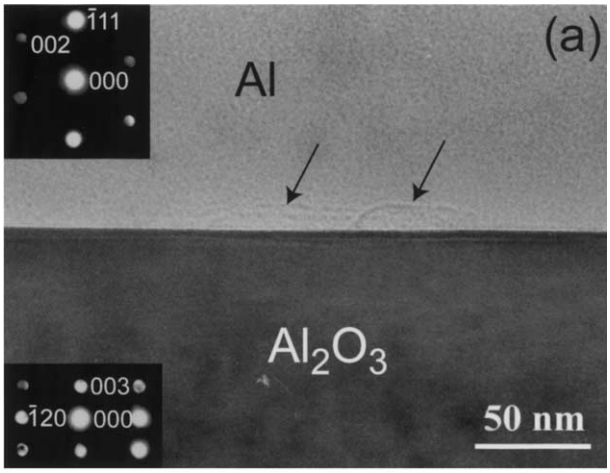

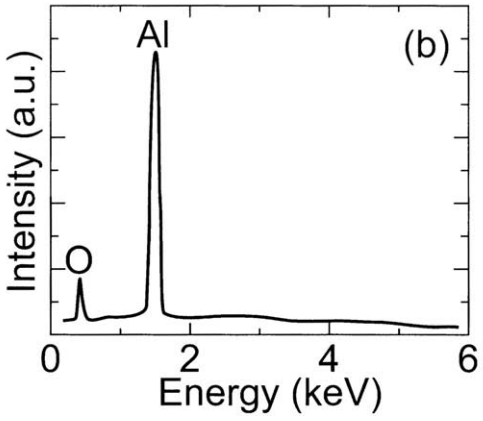

Fig. 9. (a) TEM photograph of aluminum/sapphire interface joined at 650 °C, showing diffraction patterns. The two arrows point to the distorted region in the aluminum. (b) EDX spectra from the distorted region shown in (a).

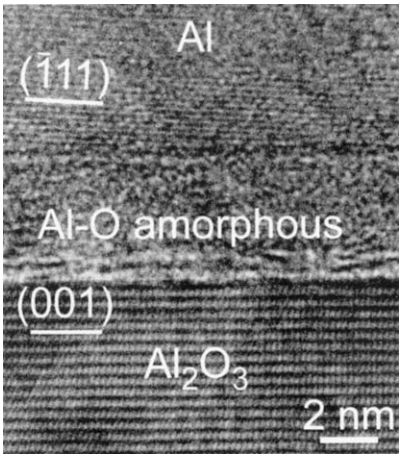

Fig. 10. HREM image of the aluminum/sapphire interface, showing an amorphous layer.

Several islands with nonuniform structure were observed attached to the interface on the aluminum side (Fig. 9a), while no corresponding feature was found on the sapphire side. Nanoprobe EDS analysis did not show any third element in these areas; only oxygen and aluminum were detected in the islands (Fig. 9b), indicating that the islands are aluminum oxide. In addition, the islands did not show any lattice fringe nor any specific diffraction spot. These islands are thus identified as amorphous aluminum oxide, which originates from the oxide skin of aluminum. A continuous amorphous alumina layer will reduce the interfacial strength,[38] but in the samples bonded above 600 °C, the amorphous material forms only isolated islands along the interface, resulting in bonds with strengths approaching that of alumina. Conversely, the presence of a continuous layer of amorphous alumina in the samples joined below 600 °C[36] results in the formation of weak interfaces.

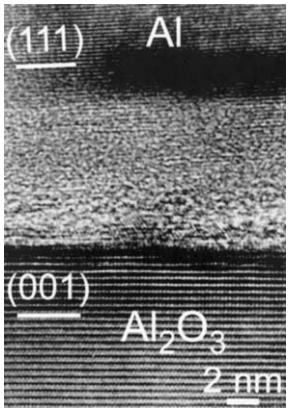

Fig. 11. HREM image of the aluminum/sapphire interface, showing lattice fringes in an amorphous layer.

High-resolution TEM reveals the formation of a new crystalline structure, shown in Fig. 11, at the interface between sapphire and the amorphous oxide. The interval of the new lattice fringes is approximately 0.20 nm, close to the lattice distance of the (002) planes of aluminum. However, nanobeam EDS clearly shows the presence of oxygen, and the crystalline phase is always in contact with the sapphire surface. These observations suggest that the crystalline phase is aluminum oxide. Fig. 12 shows a typical diffraction pattern obtained from an area with both the crystals and the sapphire substrate, as well as showing an interpretation of the diffraction pattern. Table 3 summarizes the experimentally obtained lattice distances as compared with those of aluminum and α–alumina. The experimentally obtained lattice distances correspond well to those of γ-alumina rather than to those of metallic aluminum. We conclude that the interfacial crystals in the amorphous islands are γ-alumina because, at such low temperature range, especially below 800 °C, γ-alumina is formed rather than β or α-alumina.[38–40] The fact that γ-alumina has a good orientation relationship with the sapphire substrate implies the formation of strong interfaces between the two phases. The orientation relationship between sapphire and γ-alumina can be expressed by Eq. (2), replacing aluminum with γ-alumina.

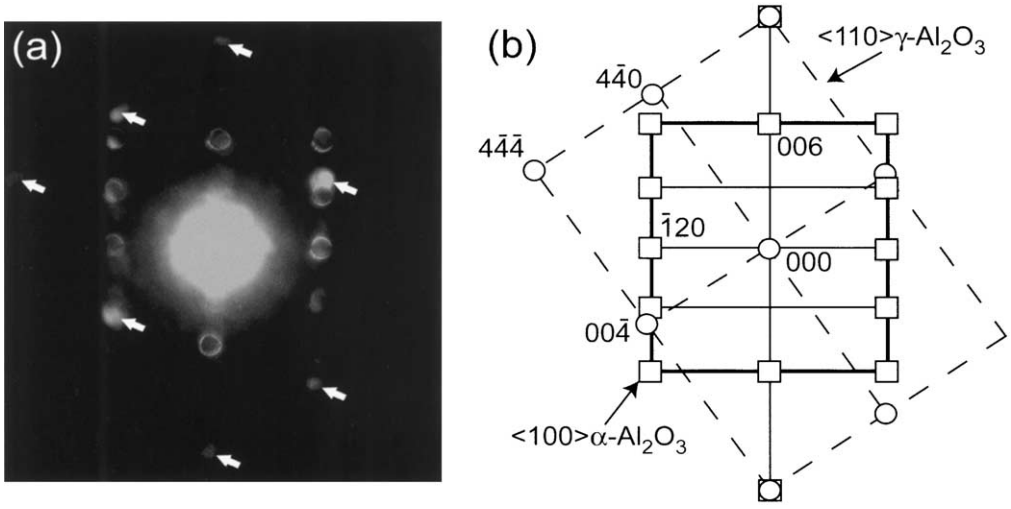

Fig. 12. (a) Diffraction pattern obtained from amorphous layer with lattice fringes near sapphire; (b) interpretation of the diffraction pattern. The arrows indicate the diffraction from the lattice in the amorphous layer.

Table 3
Lattice distances obtained from the diffraction pattern shown in Fig. 10[a]

System	Distance (nm)	
Measured	1.38	1.88
Al	1.431(002) plane	2.024(220) plane
γ-Al_2O_3	1.395(004) plane	1.977(440) plane

[a] Distances for Al and γ-Al_2O_3 are shown for comparison.

4. Conclusions

In the present work, several aspects of the Al/Al_2O_3 interfaces have been evaluated: wetting, atomic transport, anisotropy, strength, and microstructure. The results can be summarized as follows:

1. The contact angle of liquid aluminum on alumina is lower than 90° at temperatures higher than 1000 °C, and decreases with temperature to ~70° at 1500 °C.
2. Transport rates at the Al/Al_2O_3 interface and on the free surface of alumina away from the drop are much faster than previously reported for pure alumina and other metal/alumina systems.
3. The Al/Al_2O_3 interface is highly anisotropic. The basal plane of alumina seems to be one of the stable interfacial planes.
4. In solid-state joining, the strength of the joint increases with increasing temperature. In liquid-state brazing, the strength gradually decreases because of the formation of unbonded regions.
5. The strength of the bonded area, σ_b, can be expressed as a function of unbonded area, A, by the following equation: $\sigma_b = 2.69\ A + 116$ (in MPa, $70\% \leqslant A \leqslant 100\%$).
6. The highest strength (400 MPa) was obtained when the interface was formed near the melting temperature of aluminum.
7. The interfacial aluminum layer becomes a single crystal when it is joined to sapphire. The following crystallographic orientation relationship was established:

$$\left(\bar{1}11\right)_{Al}//(001)_{\alpha-Al_2O_3},\ <110>_{Al}\ //\ <100>_{\alpha-Al_2O_3}$$

8. Amorphous aluminum oxide islands formed at the interface. In the amorphous oxide, γ-alumina nanocrystals with the same orientation relationship grew from the sapphire.

Acknowledgements

K. Suganuma's work was supported by the 21COE program of The Ministry of Education, Culture, Sports, Science and Technology. E. Saiz's and A. P. Tomsia's work was supported by the Director, Office of Energy Research, Office of Basic Energy Sciences, Materials Sciences Division, of the U.S. Department of Energy under Contract No. DE-AC03-76SF00098.

References

1. Brennan, J. J. and Pask, J. A., Effect of nature of surfaces on wetting of sapphire by liquid aluminum. *J. Am. Ceram. Soc.*, 1968, **51**, 569–573.
2. Nicholas, M. G., Mortimer, D. A., Jones, L. M. and Crispin,

R. M., Some observations on the wetting and bonding of nitride ceramics. *J. Mater. Sci.*, 1990, **25**, 2679–2689.
3. Klomp, J. T., Bonding of metals to ceramics and glasses. *Am. Ceram. Soc. Bull.*, 1972, **51**, 683–688.
4. Iseki, T. and Nicholas, M. G., The elevated temperature strengths of alumina–aluminium and magnesium-aluminium samples. *J. Mater. Sci.*, 1979, **14**, 687–692.
5. Kohno, T., Yamada, T. and Yokoi, K., Bonding of ceramics to metals with interlayers of Al–Si clad aluminium. *J. Japan Inst. Metals*, 1985, **49**, 876–883.
6. Suzumura, A., Onzawa, T., Arata, Y., Ohomori, A. and Sano, S., Friction welding of ceramics to aluminum. *J. High Temp. Soc.*, 1987, **13**, 43.
7. Suganuma, K., New process for brazing ceramics utilizing squeeze casting. *J. Mater. Sci.*, 1991, **26**, 6144.
8. Levi, C. G., Abbaschian, C. J. and Mehrabian, R., Interface interactions during fabrication of Al alloy/Al_2O_3 fiber composites. *Metall. Trans. A*, 1978, **9**, 697–711.
9. Munitz, A., Metzger, M. and Mebrabian, R., The interface phase in Al–Mg/Al_2O_3 composites. *Metall. Trans. A*, 1979, **10**, 1491–1496.
10. Hall, I. W. and Barrailler, V., The effect of thermal exposure on the microstructure and fiber /matrix interface of an Al_2O_3/Al composite. *Metall.Trans.A*, 1986, **17**, 1075–1080.
11. Naidich, Yu.V, Chubashov, Yu.N, Ischchuk, N. F. and Krasovskii, V. P., Wetting of some nonmetallic materials by aluminum. *Poroshkovaya Metallurgiya*, 1983, **22**, 67–69.
12. Weirauch, D. A. Jr., A reappraisal of wetting in the system Al–Al_2O_3 from 750-1000 °C. In *Ceramic Microstructures '86. Role of Interfaces*, ed. J. A. Pask and A. G. Evans. Plenum Press, New York, 1987, pp. 329–340.
13. Champion, J. A., Keene, B. J. and Sillwood, J. M., Wetting of aluminum oxide by molten aluminum and other metals. *J. Mat. Sci.*, 1969, **4**, 39–49.
14. Kaplan, W. D., Alumina–aluminum interfaces. Non-equilibrium wetting in a binary system. In *Interfacial Science in Ceramic Joining*, ed. A. Bellosi, T. Kosmač and A. P. Tomsia. Kluwer Academic Publishers, London, 1998, pp. 153–160.
15. Levi, G. and Kaplan, W. D., Oxygen induced interfacial phenomena during wetting of alumina by liquid aluminium. *Acta Mater.*, 2002, **50**, 75–88.
16. Woohyun, Jung, Huesup, Song, Sang Whan, Park and Doh-Yeon, Kim, Variation of contact angles with temperature and time in the Al–Al_2O_3 System. *Met. & Mat. Trans. B-Process Metallurgy & Materials Processing Science*, 1996, **27B**, 51–55.
17. Laurent, V., Chatain, D., Chatillon, C. and Eustathopoulos, N., Wettability of monocrystalline alumina by aluminum between its melting point and 1273 K. *Acta Metall*, 1988, **36**, 1797–1803.
18. Ricci, E. and Passerone, A., Review: surface tension and its relations with adsorption, vapourization and surface reactivity of liquid metals. *Mat. Sci. Eng.*, 1993, **A161**, 31–40.
19. Saiz, E., Tomsia, A. P. and Cannon, R. M., Ridging effects on wetting and spreading of liquids on solids. *Acta Mater.*, 1998, **46**, 2349–2361.
20. Saiz, E., Tomsia, A. P. and Cannon, R. M., Triple line ridging and attachment in high-temperature wetting. *Scripta Materialia*, 2001, **44**, 159–164.
21. Saiz, E., Cannon, R. M. and Tomsia, A. P., Energetics and atomic transport at liquid metal/Al_2O_3 interfaces. *Acta Mater.*, 1999, **47**, 4209–4220.
22. Saiz, E., Tomsia, A. P. and Cannon, R. M., Wetting and work of adhesion in oxide/metal systems. In *Ceramic Microstructures: Control at the Atomic Level*, ed. A. P. Tomsia and A. M. Glaeser. Plenum Press, New York, 1998, pp. 65–82.
23. Keene, B. J., Review of data for the surface tension of pure metals. *Int. Mat. Rev.*, 1993, **38**, 157–192.
24. Hoffman, D. W. and Calm, J. W., A vector thermodynamics for anisotropic surfaces. I. Fundamentals and applications to plane surface junctions. *Surf. Sci.*, 1972, **31**, 368–388.
25. Herring, C., The use of classical macroscopic concepts in surface-energy problems. In *Structure and Properties of Solid Surfaces*, ed. R. Gomer and C. S. Smith. University of Chicago Press, Chicago, 1953, pp. 5–72.
26. Mullins, W. W., Theory of thermal grooving. *J. Appl. Phys*, 1957, **28**, 333–339.
27. Mullins, W. W., Grain boundary grooving by volume diffusion. *Trans. Met. Soc. AIME*, 1960, **218**, 354–361.
28. Wriedt, H. A., The Al–O (aluminum–oxygen) system. *Bull. Alloy Phase Diagrams*, 1985, **6**, 548–553.
29. Jung-Hae, Choi, Doh-Yeon, Kim, Hockey, B.J, Wiederhom, S. M., Handwerker, C. A., Blendell, J. E., Carter, W. C. and Roosen, A. R., Equilibrium shape of internal cavities in sapphire. *J. Am. Ceram. Soc.*, 1997, **80**, 62–68.
30. Kitayama, M. and Glaeser, A. M., The energetics and kinetics of pore shape changes in alumina. *Key Eng. Mat.*, 1999, **159-160**, 193–204.
31. French, T. M. and Somorjai, G. A., Composition and surface structure of the 0001 face of α-alumina by low-energy electron diffraction. *J. Phys. Chem.*, 1970, **74**, 2489–2495.
32. Gautier, M., Renaud, G., Van, L. P., Villette, B., Pollak, M., Thromat, N., Jollet, F. and Duraud, J-P., α Al_2O_3/(0001) surfaces: atomic and electronic structure. *J. Am. Ceram. Soc.*, 1994, **77**, 323–334.
33. Kruzic, J. J., Interfacial and Near Interfacial Crack Growth Phenomena in Metal Bonded Alumina. Phd thesis, University of California Berkeley, 2001.
34. Daigleish, B. J., Saiz, E., Tomsia, A. P., Cannon, R. M. and Ritchie, R. O., Interface formation and strength in ceramic-metal systems. *Scripta Met. Mat*, 1994, **31**, 1109–1114.
35. Hansen, M., *Constitution of Binary Alloys*. McGraw-Hill Book Co., Inc, New York, 1958.
36. Klomp, J. T., Ceramic and metal surfaces in ceramic-to-metal bonding. *Proceedings of the British Ceramic Society*, 1984, **34**, 249–259.
37. Fecht, H. J. and Gleiter, H. A., Lock-in model for the atomic structure of interphase boundaries between metals and ionic crystals. *Acta Metall*, 1985, **33**, 557–562.
38. Ikeuchi, K., Solid state bonding of aluminum alloys to dissimilar metals. *J.Japan Inst. Light Metals*, 1996, **46**, 298–306.
39. Suganuma, K., Interfaces in β-SiC whiskers/6061 aluminum composites. *J. Mater. Res.*, 1993, **8**, 2569–2576.
40. Suganuma, K., Interfacial microstructures of potassium titanate whiskers in pure aluminum and 6061 alloy matrix. *J. Japan Inst. Metals*, 1994, **58**, 1213–1219.